Eur. Phys. J. Appl. Phys. **31**, 169–178 (2005)
DOI: 10.1051/epjap:2005055

THE EUROPEAN PHYSICAL JOURNAL
APPLIED PHYSICS

Instability analysis of charges trapped in the oxide of metal-ultra thin oxide-semiconductor structures

A. Aziz[1], K. Kassmi[1,a], R. Maimouni[1], F. Olivié[2], G. Sarrabayrouse[2], and A. Martinez[2]

[1] Université Mohamed Premier, Faculté des Sciences, Dépt de Physique, (L.E.A.A), route Sidi Maafa, BP 524, Oujda, Morocco
[2] Laboratoire d'Analyse et d'Architecture des Systèmes (LAAS-CNRS), 7 avenue du colonel Roche, 31077 Toulouse, France

Received: 11 November 2004 / Received in final form: 26 April 2005 / Accepted: 17 May 2005
Published online: 14 September 2005 –

Abstract. In this paper, we present the theoretical and experimental results of the influence of a charge trapped in ultra-thin oxide of metal/ultra-thin oxide/semiconductor structures (MOS) on the $I(Vg)$ current-voltage characteristics when the conduction is of the Fowler-Nordheim (FN) tunneling type. The charge, which is negative, is trapped near the cathode (metal/oxide interface) after constant current injection by the metal ($Vg < 0$). Of particular interest is the influence on the $\Delta Vg(Vg)$ shift over the whole $I(Vg)$ characteristic at high field (greater than the injection field (>12.5 MV/cm)). It is shown that the charge centroid varies linearly with respect to the voltage Vg. The behavior at low field (<12.5 MV/cm) is analyzed in référence A. Aziz, K. Kassmi, Ka. Kassmi, F. Olivié, Semicond. Sci. Technol. 19, 877 (2004) and considers that the trapped charge centroid is fixed. The results obtained make it possible to analyze the influence of the injected charge and the applied field on the centroid position of the trapped charge, and to highlight the charge instability in the ultra-thin oxide of MOS structures.

PACS. 73.40.Qv Metal-insulator-semiconductor structures (including semiconductor-to-insulator)

1 Introduction

Degradation of the metal-ultra thin oxide-semiconductor structure (MOS), due to the injection of carrier effect, leads to the creation of interface states and the formation of charges in the oxide. These interfacial and bulk charges produce instability of the MOS devices. Analysis and control of these degradations with a view to optimizing these devices is of great importance [1–7].

In previous studies [1], we analyzed the theoretical influence of negative charges trapped in the oxide on $I(Vg)$ characteristics where the conduction is of the Fowler-Nordheim (FN) type [8–13]. We found that by maintaining a constant current the ΔVg shift depends on the Vg voltage and on the position of the centroid (X_b) with respect to the tunnel distance (X_t). ΔVg increases when charges are located inside the tunnel distance, and remains constant when the charges are outside. These results are validated experimentally using the $I(Vg)$ ($Vg < 0$) characteristics, obtained after constant current injection ($Vg(Q_{\text{inj}})$, Q_{inj}: injected charges), at low field (lower than the injection field (<12.5 MV/cm)). From the characteristics $Vg(Q_{\text{inj}})$, we determined the rate (R) of creation of the charge trapped in the oxide and the charge density after several injection stages. Modeling of the $I(Vg)$ characteristics enables to show that the trapped charge centroid (X_b) moves toward the cathode (metal/oxide interface) when the injection charge increases.

In the literature, [14–16] reviewed the trapping of charges in the oxide with respect to the injection field. For fields greater than 3 MV/cm, it has been shown [14], using optical methods, that the negative charge centroid moves toward the cathode when the field increases. This is due to the trapping of electrons caused by hydrogen (H_2) centers that are diffused from anode to cathode under the electric field effect. From a first order trapping model, [15,16] investigated the spatial distribution of negative charges in the oxide with respect to the injection field. When the field increases, the trapping of negative charges is most important near the cathode. This is due to the detrapping of the electrons, which are near the anode, by the presence of a high field effect at this interface.

In other works, [17,18] reported the instability of negative charges trapped in the oxide. Some charges are detrapped after injection interruption and a discontinuity may occur at the beginning of the next injection.

In the literature, no mention is made of the trapped charge analysis on the $I(Vg)$ characteristics at high field. To understand the influence of the field on the charge

[a] e-mail: khkassmi@yahoo.fr, kassmi@sciences.univ-oujda.ac.ma
This work has been partly supported by:
• le comité Franco-Marocain 'Action Intégrée', N° MA/03/78,
• le Programme Thématique d'Appui à la Recherche Scientifique (PROTARS III), N° D43/06.

centroid trapped in the oxide of MOS structures, a theoretical and experimental investigation of the $I(Vg)$ characteristics ($Vg < 0$) is carried out. Experimentally, charges are trapped in the oxide after FN constant current injection ($Vg < 0$). In our study, we focused on the modeling of the experimental $\Delta Vg(Vg)$ characteristics at high field (greater than the injection field (>12.5 MV/cm)). In the theoretical section, we analyze the charge influence on $I(Vg)$ at high and low fields. The MOS structures exhibit an oxide thickness of about 110 Å.

These results enable us to study the influence of the charge centroid position on voltage shifts ΔVg, and to supervise the evolution of this position with respect either to the injected charge at a constant current, or to the field applied by a ramp voltage $I(Vg)$. Given these results, we tried to highlight the instability of the charges trapped in the oxide.

2 Experimental procedure

The samples are made on p-type silicon wafers, $\langle 100 \rangle$ oriented, with a doping level $1{-}3 \times 10^{15}$ cm^{-2}. The oxide layers have been obtained at 900 °C in a (HCL:O_2:N_2) ambient with composition (0.2:10:90). The area S of the capacitors is 10^{-6} cm^2. Thickness ($D_{\rm ox}$) of the oxide layers is obtained from the capacitor-voltage $C(V)$ characteristics, at high and low frequencies (1 MHz and 1 kHz). Measurements were made with an impedance analyzer HP 4192A (Hewlett-Packard).

Current-Voltage ($I(Vg)$) measurements, with a ramping rate of about $15 \times 10^6 D_{\rm ox}$ V s^{-1} (with $D_{\rm ox}$ in cm), and constant current stressing ($Vg(Q_{\rm inj})$, $Q_{\rm inj}$: injected charges) have been performed using a HP 4145A semiconductor parameter analyzer. In our experiment, current injection corresponds to a field of 12.5 mV/cm. The $I(Vg)$ measurements have been carried out in the medium sampling mode and the constant current injection in the fast sampling mode.

3 Results and discussion

3.1 Theoretical results

3.1.1 Fowler-Nordheim conduction in the presence of localised charges in the oxide

Physical models of MOS structures have been developed using the energy band diagram, presented in Figure 1. In this study, the conduction FN including the localized charges trapped in the oxide is investigated.

In the case of injection by tunnel effect, the probability of transmission for electrons of energy E_x, is given by [8,9,19]:

$$T(E_x) = \exp\left(-2\int_{X=0}^{X_{tx}} k(x)dx\right) = \exp\left(-2\int_{X=0}^{X_{tx}} \sqrt{\frac{2m_0^*}{\hbar^2}\left(q\psi(x) - E_x\right)}dx\right) \quad (1)$$

where:

E_x: the energy (E) component perpendicular to the barrier,

X_{tx}: tunnel distance in the oxide for an electron with energy (E_x) (Fig. 1),

m_0^* : effective mass of the electron in the oxide, $\hbar$: the reduced Plank constant,

q: electron charge, $q\Psi(x)$: potential barrier in the oxide.

The FN tunnel current density ($J_{\rm FN}$), which crosses the structure, is obtained by adding all possible E_x energies. It is given by the expression [7,8,19]:

$$J_{\rm FN} = \frac{4\pi q m_o}{h^3}\int_{E_x} T(E_x)\,dEx \int_{E_x}^{\infty} f(E,T)dE \quad (2)$$

where, m_0: mass of the free electron, $f(E,T)$: Fermi-Dirac's distribution depending on temperature (T) [11,12,20].

In the case of a trapped charge with a density N_1 at $x = X_b$, the potential barrier ($q\psi(x)$) distribution can be easily obtained by solving the Poisson equation:
if $0 \le x \le X_b$:

$$q\psi(x) = -\frac{q}{\varepsilon_o\varepsilon_{ox}}(N_1.x) + qE_2x + q\psi(o) \quad (3)$$

if $X_b \le x \le D_{ox}$:

$$q\psi(x) = -\frac{q}{\varepsilon_o\varepsilon_{ox}}(N_1.X_b) + qE_2x + q\psi(o) \quad (4)$$

with: $\varepsilon_o(\varepsilon_{ox})$: permittivity of vacuum (the oxide), E_2: interfacial field in the oxide at oxide/semiconductor interface (anode), it is calculated following the procedure described in [12], $q\psi(o)$: metal/oxide interfacial barrier, here it is equal to 3 eV [11,13].

Taking into account equations (3,4), the transmission probability $T(E_x)$ for an electron energy E_x can be expressed, as a function of the electrical field (E_1) [1] in the oxide near the cathode, as follows:

– if the charge centroid is localized in the tunnel distance ($X_{tx} > X_b$):

$$T(E_x) = \exp\left[-\frac{4}{3}\frac{(2m_{ox}q)^{1/2}}{\hbar E_1}\left\{\left(\phi_m - \frac{E_x}{q}\right)^{3/2} + \left(\frac{qN_1}{\varepsilon_{ox}E_1 - qN_1}\right)\left(\phi_m - E_1X_b - \frac{E_x}{q}\right)^{3/2}\right\}\right] \quad (5)$$

– if the charge centroid is localized outside the tunnel distance ($X_{tx} < X_b$):

$$T(E_x) = \exp\left[-\frac{4\,(2m_{ox}q)^{1/2}}{3\hbar E_1}\left(\phi_m - \frac{E_x}{q}\right)^{3/2}\right] \quad (6)$$

Equations (1–6) yield the potential barrier distribution in the oxide, the transmission probability $T(E_x)$ and then

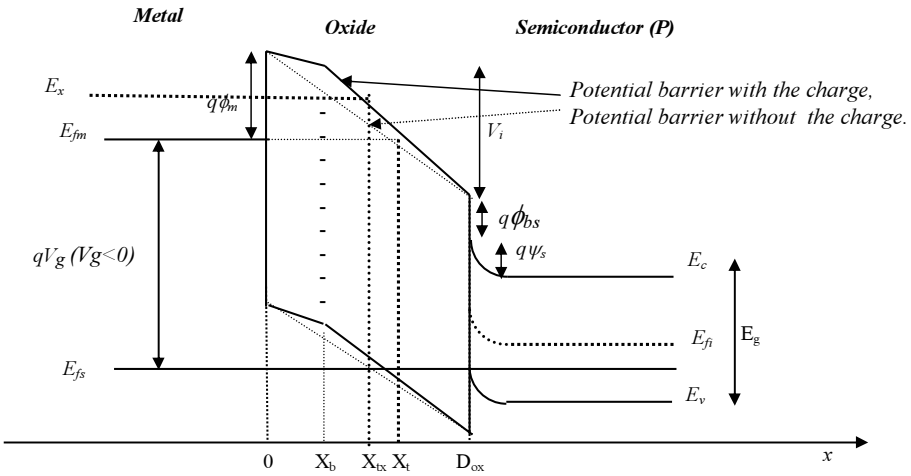

Fig. 1. Energy band diagram of MOS structures with and without of the negative charge of density N_1 situated at $x = X_b$ in the oxide for a given voltage Vg, where

Vg : applied voltage,
V_i : potential across the oxide,
ψ_s : potential surface,
$q\Phi_m$: potential barrier at metal/oxide interface,
$q\Phi_{bs}$: potential barrier at oxide/semiconductor interface,
E_{fm} : metal Fermi level,
E_{fs} : semiconductor Fermi level,
E_{fi} : intrinsic Fermi level in the semiconductor,
$E_c(E_v)$: conduction (valence) band bottom (top) in the semiconductor,
Eg : band gap of the semiconductor,
D_{ox} : oxide thickness,
x : x-axis abscissa,
X_t : tunneling distance at constant current,
X_{tx} : tunneling distance for electron energies of E_x for a given voltage Vg.

the current density J_{FN}. This computation is effected numerically, by taking the origin of energies as Fermi's energy (E_{fm}) of the metal.

In [1] we analyzed the charge influence on $I(Vg)$ characteristics (at low field) when the centroid (X_b) is fixed. At high field, the charge centroid depends on the injected charge and on the injection field [5,6,14–16]. This will be clarified in the next sections where the theoretical influence of the centroid displacement on the $I(Vg)$ characteristics will be investigated. Based on the experimental results (Sect. 3.2.2), the centroid displacement with respect to Vg voltage is supposed to be of the form:

$$X_b = A + B.Vg \tag{7}$$

where, A and B: coefficients depending on the current injection (field, injected charges).

For a displacement from the cathode (metal) toward the anode (Si), the value of (B) factor is positive but in the reverse direction, it is negative.

3.1.2 Influence of the trapped charge on the *I(Vg)* characteristic

Figure 2 shows the typical calculated influence of the charge centroid displacement (from cathode to anode and vice-versa) on the shift ΔVg, with respect to the Vg voltage. In both cases the shift ΔVg depends on the voltage Vg and on the B factor. To account for this behavior, Figure 3 shows, according to voltage Vg, the characteristics $\Delta Vg(X_b)$ in the case of a fixed centroid (continuous line) [1] and a mobile centroid (Fig. 2). Thus, one can conclude by taking account the result obtained in [1] (see introduction), that:

- ΔVg increases with voltage Vg when charges move from the cathode to the anode inside the tunnel zone (that part of Fig. 2A curve where ΔVg varies with Vg for a given X_b value), or from the anode toward the cathode when the charges move outside the tunnel zone (that part of Fig. 2B curve where ΔVg does not vary with Vg for a given X_b value).
- ΔVg decreases with the voltage Vg, when charges move toward the anode outside the tunnel zone, or toward the cathode inside the tunnel zone.
- ΔVg reaches a peak in both cases when charges move close to the tunnel distance.

These interesting results enable us to localize the centroid movement from the behavior of the characteristics $\Delta Vg(Vg)$.

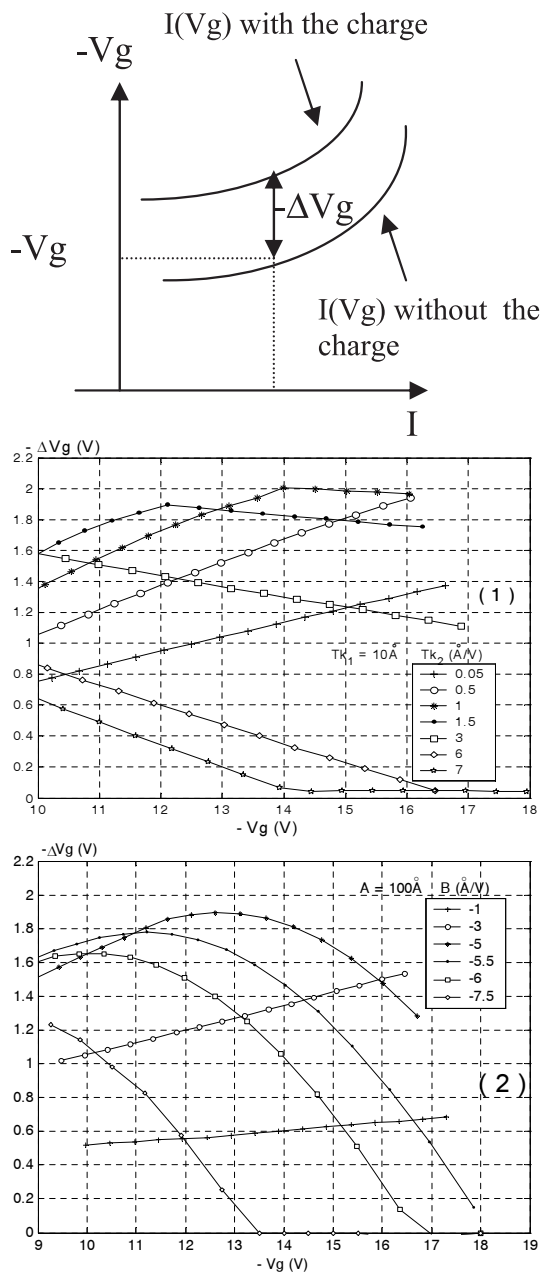

Fig. 2. Typical centroid calculated displacement influence of a negative charge of density 5×10^{12} cm^{-2}on the $\Delta Vg(Vg)$ characteristics (see insert figure). $\phi_m = 3$ eV, $D_{\text{ox}} = 110$ Å.
(1) Yields the displacement of the negative charge centroid toward the anode.
(2) Yields the displacement of the negative charge centroid toward the cathode.

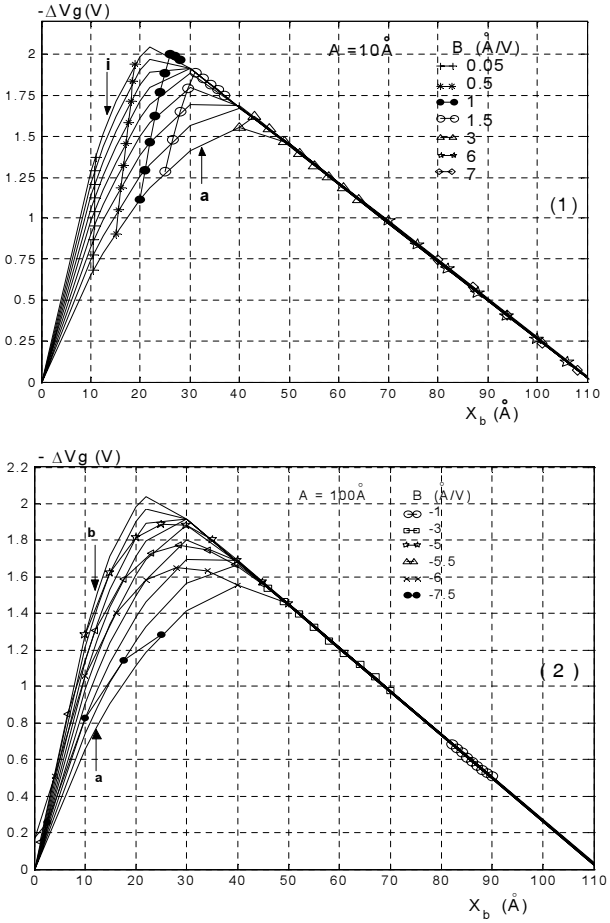

Fig. 3. Typical calculated influence of the centroid of a negative charge of density 5×10^{12} cm^{-2} on the ΔVg shift with respect to the voltage (Vg). $\phi_m = 3$ eV, $D_{ox} = 110$ Å.
——— : (Continuous line) case of a charge centroid independent of the Vg voltage [1]. $Vg(V)$: (a) −10, (b) −11, (c) −12, (d) −13, (e) −14, (f) −15, (g) −16, (h) −17, (i) −18 (intermediate curves (b–h) are situated between the terminal curves a and I respectively).
(1) Yields the displacement of the negative charge centroid toward the anode.
(2) Yields the movement of the negative charge centroid toward the cathode.

3.1.3 Influence of charge trapped in the oxide on the apparent barrier (Φ_m^{ch})

The influence of the trapped charge displacement on the apparent barrier (Φ_m^{ch}), computed as shown in [1,11,13,21] at high field (12−14 MV/cm) and low field (8−12 MV/cm) from the FN plot, is given in Figure 4. It reveals different behaviors when the charges move in both directions and particularly for high values of parameter B. Comparing these curves with those of Figure 3, it can be concluded that:

– When the charges move toward the anode inside and outside the tunnel distance, the effect on the apparent barrier increases and decreases respectively. This effect is maximum when the tunnel distance is close to the charge centroid.
– When charges move toward the cathode, the effect on the barrier increases particularly when the charges move near the cathode inside the tunnel distance. When the centroid (X_b) moves toward the cathode inside the tunnel distance from 30 Å to 10 Å ($B = -6$ Å/V), the apparent barrier (Φ_m^{ch}) increases by 38% for a charge density ($N_1 = 5 \times 10^{12}$ cm^{-2}).

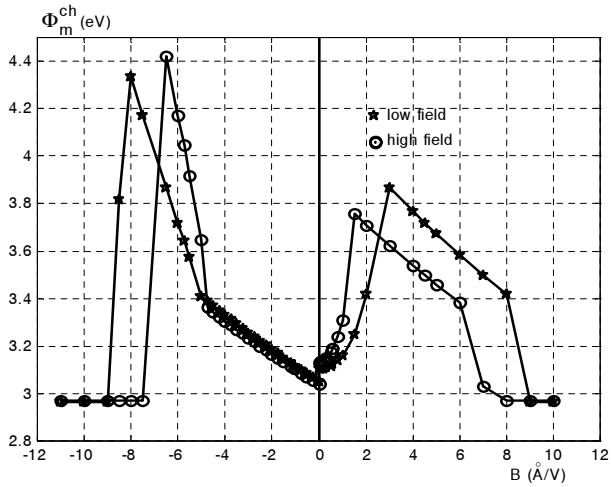

Fig. 4. Centroid movement influence of a negative charge of density 5×10^{12} cm^{-2} on the apparent barrier (Φ_m^{ch}) at low and high field. $\phi_m = 3$ eV, $D_{ox} = 110$ Å.

– When the factor (B) reaches high values, the effect on the apparent barrier (Φ_m^{ch}) is negligible, because the charge centroid is situated at one of the interfaces.

3.2 Experimental results

3.2.1 Influence of trapped charges on *I(Vg)* characteristics

After injecting currents of variable durations, we plotted the $Vg(Q_{\rm inj})$ characteristic sequences obtained in Figure 5 and $I(Vg)$ characteristics ($Vg < 0$) in Figure 6 after eliminating the excess current occurring at low field [1,11,13]. It seems that there is negative charge trapping as shown by a shift of the characteristics $Vg(Q_{\rm inj})$ and $I(Vg)$ toward negative voltages.

From the characteristics of Figure 6, we plotted in Figure 7 the ΔVg shift as a function of Vg after each injection. The following behavior patterns can be noted:

– For voltages lower than those corresponding to the injection current (<13.5 V), the $\Delta Vg(Vg)$ shift depends on the injected charge. It is constant for charge densities lower than 7 C/cm^2 and increases with the voltage when injected charge densities are more than 7 C/cm^2. As mentioned in Section 1, the behavior of these characteristics has been interpreted as follows [1]: at low (high) injected charge, the negative charges are trapped outside (inside) the tunnel distance. We modeled these characteristics, by fixing the trapping parameters (negative charge density and centroid), listed in Table 1. Clearly a good agreement can be found between theory and experiment. These results show that the negative charge centroid depends on the injected charge in the oxide. When the injected charge increases, the negative charges are trapped increasingly closer to the cathode. The movement of trapped charge centroid toward the cathode may be interpreted as follows: when the injected charge increases, the density of the trapped negative charge in the oxide increases, this leads to a reduction of the field at the cathode and to its increase at the anode. Thus, under the effect of this field, the electrons trapped near the anode are detrapped and the negative charge centroid moves toward the cathode.
– For voltages greater than those corresponding to the injection current (>13.5 V), there exits a decrease of ΔVg with the Vg voltage, for each current injection. These characteristics are analyzed in the following paragraph.

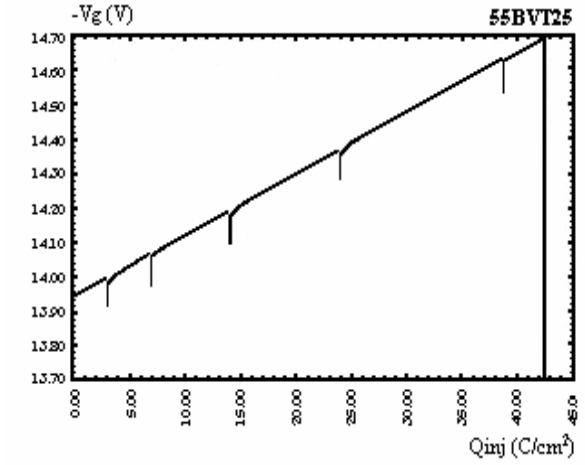

Fig. 5. Typical $Vg(Q_{\rm inj})$ characteristic sequences obtained after current injection to breakdown, $D_{ox} = 109$ Å, $S = 10^{-6}$ cm^2, $I = 10^{-8}$ A.

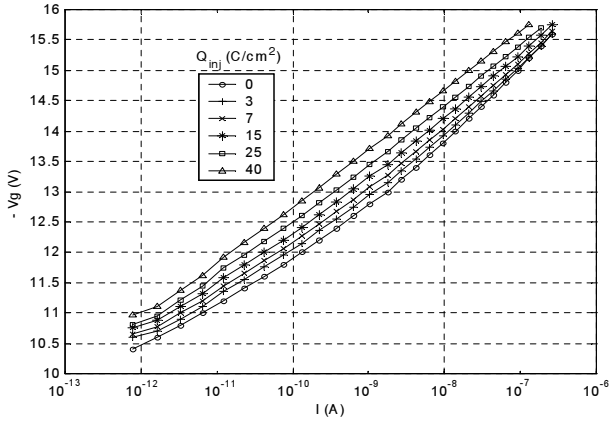

Fig. 6. Typical influence of constant current injection corresponding to that of Figure 5 on $I(Vg)$ characteristic ($Vg < 0$) obtained after removing the excess current at low field [1,13].

3.2.2 Analysis of the $\Delta Vg(Vg)$ at high field ($-Vg > 13.5$ V)

The plot of ΔVg with respect to Vg shown in Figure 7 exhibits different behaviors at high field ($-Vg > 13.5$ V) with respect to that at low field ($-Vg < 13.5$ V). The

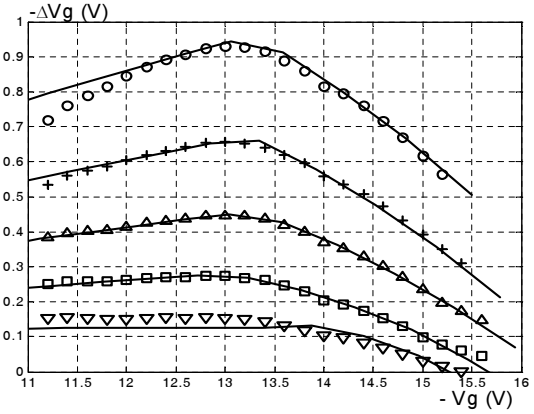

Fig. 7. Typical $\Delta Vg(Vg)$ characteristics obtained from Figure 6 after each current injection. experiment: $Q_{\rm inj}$ (C/cm^2): (∇) 3, ($\Box$) 7, ($\triangle$) 15, (+) 25, (o) 40.
(——) theory:
• $-Vg < 13.5$ V, for a fixed charge centroid by taking account the trapping parameters listed in Table 1 [1],
• $-Vg > 13.5$ V, for a displacement charge centroid toward the cathode taking account of the trapping parameters listed in Table 2.

Table 1. Trapping parameters, negative charges density and centroid allowing to model the $\Delta Vg(Vg)$ characteristic at low field ($-Vg < 13.5$ V) [1].

$Q_{\rm inj}$ (C/ cm^2)	X_b (Å)	N_1 (cm^{-2})
3	31.5	3.4×10^{11}
7	22.5	7.0×10^{11}
15	14.5	1.7×10^{12}
25	12.5	2.8×10^{12}
40	10.75	4.5×10^{12}

ΔVg shift decreases with the Vg voltage after each injection. From a critical voltage, corresponding to that of the injection current, the experimental characteristics deviate from the theoretical ones computed by taking into account a fixed centroid of negative charges (Tab. 1).

Compared with theoretical results, the high field decrease may be modeled by considering:

(a) the influence of a fixed positive charge in the oxide,
(b) the detrapping of negative charges during the acquisition $I(Vg)$ characteristics,
(c) the movement of the negative charges toward the anode or cathode when Vg increases.

In the following paragraphs these assumptions are reviewed.

3.2.2.1 Analysis of positive charge trapped in the oxide

With respect to (a) we tried to model the decreasing part by taking a fixed positive charge in the oxide at several positions. Nevertheless, we were unable to model the $\Delta Vg(Vg)$ after each injection. Furthermore, to confirm the non validity of the positive charge model, we experimentally reviewed the influence of maximum voltage (Vgmax) of the second passage $I(Vg)$ characteristic (Fig. 8), obtained after injecting a constant current, on the third passage $I(Vg)$ characteristic. Clearly, the third passage $I(Vg)$ depends on the Vgmax. When Vgmax is about -15.7 V and when meets the first characteristic then the third passage $I(Vg)$ is the same as the first one (without charge) (Fig. 8B). This shows that after the second $I(Vg)$ passage at high field, the charges trapped in the oxide are either detrapped or move toward the interfaces. Thus if it were due to the positive charge trapping then as it occurs during the third passage, the $I(Vg)$ characteristic obtained should be identical to that of the second passage; but this is not the case.

3.2.2.2 Analysis of detrapping of negative charges in the oxide

With respect to (b), to analyze the detrapping of negative charges, we plotted in Figure 9 the $\Delta Vg(Vg)$ shift corresponding to $I(Vg)$ characteristics in Figure 8A. From the third passage, the $\Delta Vg(Vg)$ characteristics obtained remain identical to that obtained at the third passage. The ΔVg increases for voltages lower than 13.5 V and gets closer to the maximum value of the second characteristic. From the critical voltage 13.5 V the high field phenomenon is repeated. Also, we verified that:

– trapping that occurs during the phase of recording the $I(Vg)$ characteristic is almost negligible,
– after injecting a constant current at high field, a major trapping of negative charges occurs [10,12] which is highlighted by the increase of shift ΔVg of $\Delta Vg(Q_{\rm inj})$ characteristics.

If detrapping occurs at high field then, from the third passage, the ΔVg will not increase with the Vg voltage, and will almost reach the maximum value of the second $I(Vg)$ characteristic. Furthermore, we must have to observe a small effect of trapped charges on the third characteristic. This contradicts the effect of negative charge detrapping at high field. Also, it is reasonable to think that the curve 3 in Figure 8A is obtained by filling the centers from which electrons have been detrapped when the $I(Vg)$ is being taken in the second passage. However, this cannot be the case because in Figure 8B the third and first $I(Vg)$ characteristic match. This excludes the filling of the latter centers while taking the third $I(Vg)$ characteristics, and shows that the high biasing of the second $I(Vg)$ may only move the charges toward the interfaces.

Curve 3 in Figure 8B can be interpreted by the displacement of charges during acquisition of the second $I(Vg)$ characteristics outside the oxide layer.

3.2.2.3 Analysis of centroid displacement in the oxide

With respect to (c) as mentioned in the theoretical section, the same effect is obtained on the $I(Vg)$ characteristics when charges move toward the cathode or anode. However, in our case, where the charge centroid is located near the cathode inside the tunnel distance, the direction

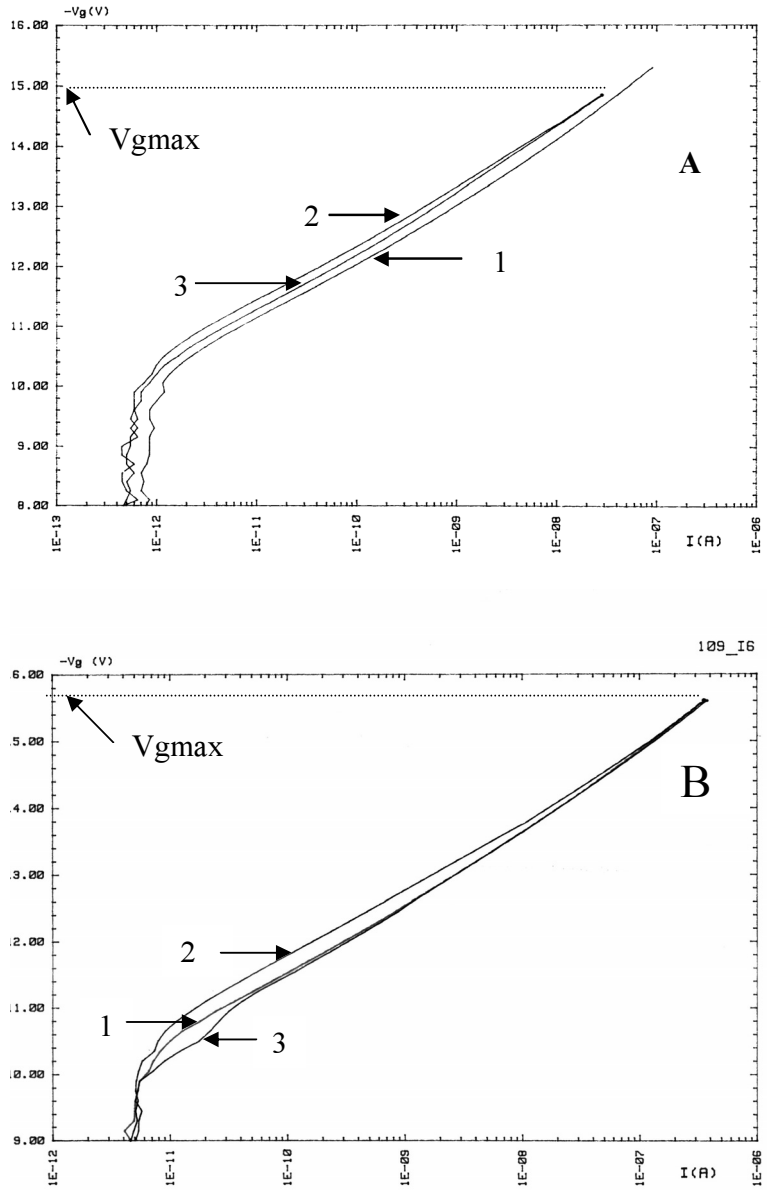

Fig. 8. Typical influence of the voltage (Vgmax), fixed by the second $I(Vg)$ characteristic on the third one. D_{ox} = 109 Å, $S = 10^{-6}$ cm^2, $I = 10^{-8}$ A. Vgmax (V): (A) –15, (B) –15.7. (1) $I(Vg)$ first passage (before injection), (2) $I(Vg)$ second passage (after injection), (3) $I(Vg)$ third passage.

difference can be obtained by computing the slope or effective barrier (Φ_m^{ch}) from the FN plot. From the plot of the effective barrier at high field ($-Vg > 13.5$ V) with respect to injected charge (Fig. 10), it can be concluded that the Φ_m^{ch} barrier increases with the injected charge up to 26%. In our experiment, this cannot be interpreted by considering the displacement of charge centroid toward the cathode, because it can also be due to an increase in charge density in the oxide after each injection.

By modeling of experimental $\Delta Vg(Vg)$ characteristics, we concluded that during acquisition of the $I(Vg)$ characteristics at high field ($-Vg > 13.5$ V), the charge centroid should be moved inside the tunnel distance toward the cathode. For each current injection and for modeling the $\Delta Vg(Vg)$ characteristics we checked that the centroid movement varies linearly with the voltage (Vg) according to equation (7). We also checked that the behavior of $\Delta Vg(Vg)$ characteristics cannot be modeled by taking account the displacement of charge centroid toward the anode. If the centroid moves toward the anode, the shift ΔVg must be increased with respect to Vg voltage.

From equations (1–7), we modeled the experimental $\Delta Vg(Vg)$ characteristics at high field (Fig. 7) by considering the parameters of Table 2. Clearly there exits a good agreement between theory and experiment. The decrease of ΔVg at high field can, therefore, be interpreted as a charge centroid movement toward the cathode. This evidences the charge instability in the oxide: the negative

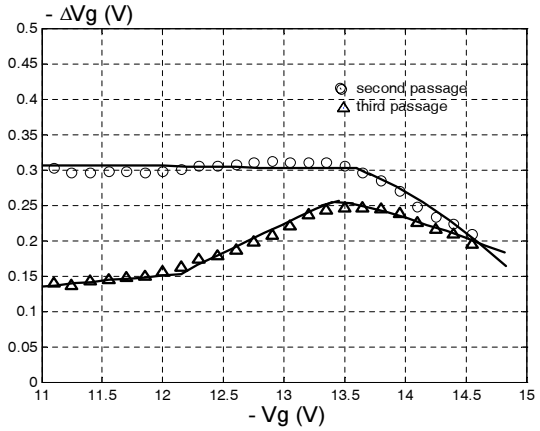

Fig. 9. Modelling of experimental $\Delta Vg(Vg)$ characteristics of Figure 8A.
(o) second passage, (△) third passage. (o, △): Experience. (——): Theory. The charge characteristics (density, centroid, ...) are given in Section 3.2.3.2.

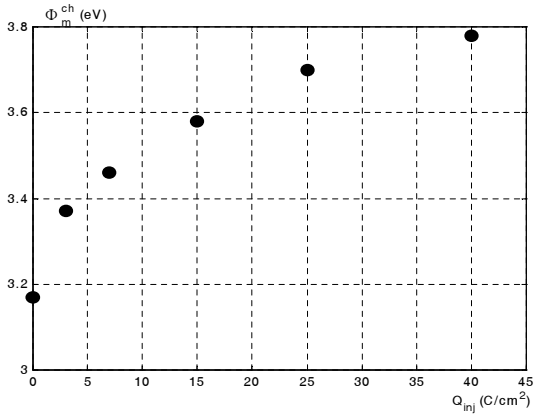

Fig. 10. Injected charge influence on the effective barrier determined from FN plot at high field ($-Vg > 13.5$ V). $D_{ox} = 109$ Å, $S = 10^{-6}$ cm^2, $I = 10^{-8}$ A.

charge centroid depends on the voltage or the applied field. In our experiment case, charges are trapped at a field of 12.5 MV/cm, and we checked that when it is greater than this critical value, charges move toward the cathode and their effect is reduced. Dependence of X_b on electrical field may be accounted for by the fact that the high field near the anode, detraps negative charges at this interface. These charges only marginally contribute to the conduction, so the X_b centroid moves toward the cathode. Detrapping electrons can be seen at high field between the second and third passages in Figure 9 with a voltage of 13.5 V.

3.2.3 Instability of the negative charges trapped in the oxide

3.2.3.1 Relaxation of trapped negative charges after constant current injection

To study the instability of negative charges trapped in the oxide, we analyzed the data of the $I(Vg)$ and $Vg(Q_{\rm inj})$ characteristics after each injection. Analysis of $Vg(Q_{\rm inj})$ characteristics shift, experimental and theoretical (considering a fixed centroid of negative charge (Tab. 1)) $I(Vg)$ characteristics shift ensuring a constant current, shows after each injection of constant current:

- the same shift for experimental $I(Vg)$ and $V(Q_{\rm inj})$ characteristics,
- the difference between experimental and theoretical shift is less than 16%.

Table 2. Parameters allowing to model the $\Delta Vg(Vg)$ characteristic at high field ($-Vg > 13.5$ V).

$Q_{\rm inj}$ (C/cm^2)	A (Å)	B (Å/V)
3	294.30	−19.21
7	142.35	−9.06
15	91.16	−5.60
25	76.50	−4.60
40	62	−3.60

Table 3. $Vg'_{\rm fnexp}$ and X'_b values obtained fo each $I(Vg)$ experiment at the constant current of 10^{-8} A.

$Q_{\rm inj}$ (C/cm^2)	$-Vg'_{\rm fnexp}$ ($I = 10^{-8}$ A)	X'_b (Å)
3	13.946	26.608
7	14.054	15.103
15	14.224	11.533
25	14.417	10.195
40	14.680	9.195

As shown in Figure 7, injection stages are located on the unstable side (decrease of ΔVg with Vg). Table 3 presents the $Vg'_{\rm fnexp}$ voltage values which maintain a constant current 10^{-8} A for each $I(Vg)$ experiment and the negative charge centroid values X'_b computed by equation (7) using the voltage $Vg'_{\rm fnexp}$ and the parameters of Table 2. The value of fixed negative charge centroid at low field (Tab. 1) and high field (Tab. 3) respectively, shows a different value particularly for a low injected charge. Since the same shifts are obtained on the $I(Vg)$ and $Vg(Q_{\rm inj})$ characteristics, this may be due to the instability of negative charge after current injection. If the injection is discontinued, charges relax by moving toward the anode. $I(Vg)$ measurement is then performed and when a field comes close to that of the injection, then the negative charges move in order to be trapped near the positions fixed by the $Vg(Q_{\rm inj})$ injection phases. Also, the values of centroid (X_b and X'_b) show that relaxation is dramatically reduced when charges are trapped near the cathode. Furthermore, we checked that this relaxation occurs by maintaining constant fields at the anode and at cathode. The combination of the $Vg(Q_{\rm inj})$ and $I(Vg)$, show that the charges relax toward the anode after each

Table 4. X_b'' values corresponding to $Vg\max = -15.8$ V, Vg_{ithe} theoretical initial value corresponding to constant current of 10^{-8} A, $Vg_{1\text{exp}}$ experimental initial value of $Vg(Q_{\text{inj}})$ characteristics.

$Q_{i\text{nj}}$ (C/cm^2)	X_b''(Å) at $Vg\max = -15.8$ V	$-Vg_{\text{ithe}}$(V) calculus at $I = 10^{-8}$ A	$-Vg_{1\text{exp}}$ (V)
3	0	13.33	13.84
7	0	13.49	13.93
15	2.68	13.66	14.09
25	3.82	13.88	14.27
40	5.12	14.16	14.53

current injection, and are trapped toward the cathode when the injected charge increases.

3.2.3.2 Instability analysis of the charges trapped in the oxide

From the successive $I(Vg)$ characteristic curves (Fig. 8A), Figure 9 shows the corresponding $\Delta Vg(Vg)$ characteristics. The behavior of second passage shows that at low field the charge centroid is located in the oxide outside the tunnel distance. At high field, this centroid moves toward the cathode when the voltage Vg increases. The parameters of charges that enable us to model the experimental $\Delta Vg(Vg)$ characteristics are:

– at low field, the charge centroid is fixed:

$$X_b = 37.5 \text{ Å}, \qquad N_1 = 8.8 \times 10^{11} \text{ cm}^2,$$

– at high field, the charge moves toward the cathode:

$$A = 161.89 \text{ Å}, B = 10.23 \text{ Å/V}, N_1 = 8.8 \times 10^{11} \text{ cm}^2,$$

In the third passage (curve 3) the characteristics obtained follow the same path. The ΔVg increases and from a critical voltage, it decreases. The third characteristic may be modeled by considering the variation of the charge centroid with respect to the voltage (Vg) as follows:

– for voltages lower than 12.5 V, the charge centroid is fixed:

$$X_b = 10 \text{ Å}, \qquad N_1 = 8.8 \times 10^{11} \text{ cm}^{-2},$$

– for voltages 12.5 V $< -Vg < 13.5$ V, the charge moves toward the anode:

$$A = -36.97 \text{ Å}, \ B = 3.81 \text{ Å/V}, \ N_1 = 8.8 \times 10^{11} \text{ cm}^{-2},$$

– for voltages greater than 13.5 V, the charge moves toward the cathode:

$$A = 99.176 \text{ Å}, \ B = -6.02 \text{ Å/V}, \ N_1 = 8.8 \times 10^{11} \text{ cm}^{-2},$$

It can be concluded that there exits a good agreement between theory and experiment. Consequently, in the second passage, the charges move toward the cathode at high field. Since the third passage, when the voltage increases, the charges move toward the anode in order to reach the charge centroid fixed by the injection field of the constant current. When we reach this field the charges move again toward the cathode. The displacement of X_b toward the anode can be accounted for as follows: when Vg increases the negative charges, detrapped near the anode during the acquisition $I(Vg)$ characteristics at high field, are trapped again near the anode and the X_b moves toward the anode.

3.2.3.3 Instability analysis associated with the beginning of the $Vg(Q_{\text{inj}})$ characteristics

The $Vg(Q_{\text{inj}})$ sequences present, as shown in Figure 5 a discontinuity at the beginning of each injection. This has previously been reported in the literature [17,18]. It has been attributed to detrapping of negative charges. To analyze this behavior, Table 4 lists:

– the negative charges centroid (X_b'') corresponding to the maximum voltage ($Vg\max = -15.8$ V) fixed by each $I(Vg)$ characteristic,
– the theoretical voltage Vg_{ithe} to maintain a constant injection current and taking into account the last charge centroid (X_b'') and charge densities N_1 of Table 1,
– the initial $Vg_{1\text{exp}}$ experimental voltage at the beginning of each injection.

These results show a disagreement between the theoretical and experimental initial voltages: the computed voltage is lower than the experiment one at the beginning of each injection. This may be due to the imprecision of the first measurements of $Vg(Q_{\text{inj}})$ characteristics, since this measurement is only performed 10 ms after the current injection. Also, the $Vg(Q_{\text{inj}})$ characteristics of Figure 5 show that at the beginning of each injection, there is a fast return to the linear part of the negative charges trapping.

Based on these results and on the modeling of the $\Delta Vg(Vg)$ after several $I(Vg)$ passages (Fig. 9), we may attribute the discontinuity of $Vg(Q_{\text{inj}})$ characteristics to a return or movement of the negative charges toward the anode to reach the charge centroid position corresponding to the injection field at a constant current. After each $I(Vg)$ characteristic, the charge centroid moves toward the cathode. So, the charge effect is reduced because charges are close to the interface. Consequently, at the next injection, the initial $Vg_{1\text{exp}}$ decreases and the centroid moves toward the anode due a major field effect.

Thus, discontinuities of $Vg(Q_{\text{inj}})$ characteristics are not due to detrapping of the negative charge as reported in the literature [17,18]; but, to the displacement of the charge toward the anode.

4 Conclusion

Modeling of the $I(Vg)$ characteristics after a current injection, by FN effect, has validated the theoretical model in the presence of a charges trapped in the oxide and evidences the charge instability.

For fields lower than that of the current injection, the $I(Vg)$ characteristics are modeled by considering that the centroid is fixed. In this case, the ΔVg shift, which maintains a constant current, depends on the charge centroid position with respect to tunnel distance. When the centroid is located inside the tunnel distance, ΔVg increases with the Vg voltage. When the centroid is outside, ΔVg is independent of Vg. These results support the view that the centroid X_b of trapped charges moves toward the cathode when the injected charge increases.

For fields greater than that of the current injection, the $I(Vg)$ characteristic is modeled by considering a voltage dependent charge centroid position. This has been made possible by supervising the centroid movement with respect to the voltage Vg or field: when Vg increases X_b moves toward the cathode. The results obtained at low and high fields enable us to conclude that:

- The charge trapped in the oxide after each injection is relaxed: when the current injection is discontinued, X_b moves toward the anode. This relaxation decreases with the injected charge.
- The charge centroid moves toward the cathode when the injected charge increases.
- When the voltage or field increases, the charges move ever closer to the cathode.

After successive passages of $I(Vg)$ characteristics, after current injection, it has been shown that from the third passage when the field increases the charges trapped in oxide move toward the anode at low field and toward the cathode at high field. These results enable us to explain the discontinuity obtained at the beginning of $V(Q_{\mathrm{inj}})$ characteristics, as expressed by the charge centroid moving toward the anode.

References

1. A. Aziz, K. Kassmi, Ka. Kassmi, F. Olivié, Semicond. Sci. Tech. **19**, 877 (2004)
2. S.J. Oh, Y.T. Yeow, Solid State Electron. **32**, 507 (1989)
3. G. Slavcheva, Solid State Electron. **33**, 837 (1990)
4. S. Elrharbi, M. Jourdain, A. Meinertz Hagen, J. Appl. Phys. **76**, 1013 (1994)
5. C. Papadas, G. Guibaudo, F. Pio, C. Monserie, G. Pananakakis, P. Mortini, C. Riva, Solid State Electron. **37**, 495 (1994)
6. C. Papadas, P. Morfouli, G. Ghuibaudo, G. Pananakakis, Solid State Electron. **34**, 1375 (1991)
7. A. Aziz, K. Kassmi, F. Olivié, Nanotechnology **15**, 237 (2004)
8. Z.A. Weinberg, J. Appl. Phys. **53**, 5052 (1982)
9. M. Lenzlinger, E.H. Snow, J. Appl. Phys. **40**, 278 (1969)
10. K. Kassmi, J.L. Prom, G. Sarrabayrouse, Solid State Electron. **34**, 509 (1991)
11. Y. Khlifi, K. Kassmi, L. Roubi, R. Maimouni, Eur. Phys. J. Appl. Phys. **9**, 239 (2000)
12. Y. Khlifi, PH.D. Thesis, Université Mohamed Premier, Oujda, Morocco, 2001, p. 33
13. Y. Khlifi, K. Kassmi, L. Roubi, R. Maimouni, Phys. Status Solidi A **182**, 737 (2000)
14. D.A. Buchanan, Appl. Phys. Lett. **60**, 216 (1992)
15. E. Avni, J. Shappir, Appl. Phys. Lett. **51**, 1857 (1987)
16. E. Avni, J. Shappir, J. Appl. Phys. **64**, 734 (1988)
17. C.L. Hung, S.A. Grot, G.SH. Gildenblat, V. Bolkhosky, Solid State Electron. **32**, 767 (1989)
18. G.Q. Lo, D.L. Kwong, K.J. Abbottand, D. Nazarian, J. Eletrochem. Sol. **140**, L16 (1993)
19. Chang-Chi, Ph.D. Thesis, Berkeley, 1984
20. S.M. Sze, *Physics of Semiconductor Devices* (J. Wiley, New York, 1981)
21. K. Kassmi, PH.D. Thesis, Toulouse (France), 1991, No. 904